PERIODICO di MINERALOGIA
established in 1930

DIPARTIMENTO
DI SCIENZE DELLA TERRA

SAPIENZA
UNIVERSITÀ DI ROMA

An International Journal of
Mineralogy, Crystallography, Geochemistry,
Ore Deposits, Petrology, Volcanology
and applied topics on Environment, Archaeometry and Cultural Heritage

Multilayer corona textures in the high-pressure ultrabasic amphibolite of Mt. Nieddu, NE Sardinia (Italy): equilibrium versus disequilibrium

Massimo Scodina [1], Gabriele Cruciani [1,*], Marcello Franceschelli [1], Hans-Joachim Massonne [2,3]

[1] Department of Geological and Chemical Sciences, University of Cagliari, S.S. 554 Cittadella Universitaria, Monserrato (CA), 09042, Italy
[2] School of Earth Sciences, China University of Geosciences, Lumo Road 388, 430074 Wuhan, China
[3] Institut für Mineralogie und Kristallchemie (closed), Universität Stuttgart, Azenbergstraße 18, D-70174 Stuttgart, Germany

ARTICLE INFO

Submitted: October 2019
Accepted: March 2020
Available on line: April 2020

* Corresponding author:
gcrucian@unica.it

DOI: 10.2451/2020PM16609

How to cite this article:
Scodina M. et al. (2020)
Period. Mineral. 89, 169-186

ABSTRACT

Rocks with coronitic textures around igneous relics of olivine and plagioclase were sampled from the ultrabasic amphibolite of Mt. Nieddu being part of the so-called Migmatite Complex of northeast Sardinia. These textures are characterized by layers of orthopyroxene and clinopyroxene around olivine, and a symplectite of clinopyroxene+ spinel and garnet around plagioclase; all these minerals were overgrown by amphibole. We applied conventional geothermobarometry and pressure-temperature (P-T) pseudosection modelling of microdomains in order to constrain the main steps of the evolution of the sampled rocks. The igneous crystallization occurred at 0.2-0.5 GPa and minimum T of 780-850 °C. Garnet is the last coronitic phase formed at estimated pressures of 1.3-1.7 GPa at 680-730 °C. As similar conditions were previously determined for the pressure peak on an adjacent rock, we conclude that during corona formation chemical equilibrium was reached probably over a much wider range than of mm-sized microdomains. Slow reaction kinetics is responsible for the partial preservation of the igneous phases.

Keywords: ultrabasic amphibolite; metamorphic evolution; corona textures; counterclockwise P-T path; Variscan Sardinia.

INTRODUCTION

In the Mt. Nieddu area, NE Sardinia, a large lensoid amphibolite body, ca. 1.5 km long in NE-SW direction and maximum width of 0.5 km, crops out within the Migmatite Complex of the Inner Zone of the Variscan Sardinian belt. This metabasite body consists of two main rock types: banded amphibolites and ultrabasic amphibolites (i.e. plagioclase-banded amphibolite and ultramafic amphibolite of Ghezzo et al., 1979). The former type is coarse-grained, dark-green, banded to massive with sporadic occurrence of centimetre-sized layers which contain millimetric porphyroblastic garnet in a matrix made up of amphibole, plagioclase, quartz, and a fine-grained symplectite of clinopyroxene and plagioclase (Scodina et al., 2019). The latter type, enclosed in the banded amphibolite lens, is a heterogeneous group of rocks characterized by a massive to weakly-schistose structure and a medium grain size of the minerals. A recent study on the banded amphibolite documented granulite-facies conditions and an anti-clockwise P-T path recorded by the compositional zoning in garnet (Scodina et al., 2019). This unusual kind of path, characterized by peak pressure conditions of 1.4 GPa at 720 °C, may be typical for rocks that belong to the lowest portion of the upper plate in a

continental collision scenario, which is here related to the Variscan orogeny (Massonne et al., 2018).

In this paper we provide new microstructural and chemical data on the coronitic assemblages that developed around igneous plagioclase and olivine in the ultrabasic amphibolites of Mt. Nieddu. We determined P-T conditions of the corona formation by an integrated approach of conventional geothermobarometry and P-T pseudosections using the effective composition of a coronitic microdomain.

The aim of this paper is to show that (i) P-T pseudosection modelling applied to the coronitic texture of Mt. Nieddu rock yield reliable P-T results and that (ii) the results are in agreement with the anti-clockwise P-T path determined by Scodina et al. (2019) on the banded amphibolite.

GEOLOGICAL SETTING

The Sardinian metamorphic basement is part of the Corsica-Sardinia microplate, a segment of the Southern European Variscan belt. This microplate was detached from Europe by the opening of the Western Mediterranean Ligurian-Provençal basin starting in the Oligocene (Séranne, 1999; Gattacecca, 2001). The basement in Sardinia consists of meta-igneous to metasedimentary sequences ranging in age from the Cambrian to the Lower Carboniferous (Carmignani et al., 1994, 2001) and has been divided into three main tectono-metamorphic zones with metamorphic grade increasing from the southern External Zone (foreland zone in Figure 1) over the central Nappe Zone to the Inner Zone in the northernmost part of Sardinia (Carmignani et al., 2001) and southern Corsica (Massonne et al., 2018). The Inner Zone is further subdivided into a southern Low to Medium-Grade Metamorphic Complex (L-MGMC) and an High-Grade Metamorphic Complex (HGMC), separated by the Posada-Asinara tectonic line, which is interpreted as a transpressive shear-belt with both sinistral and dextral shearing starting at 325-320 Ma (Carosi and Palmeri, 2002; Padovano et al., 2012; Cruciani et al., 2015 a,b,c).

The HGMC consists mainly of paragneisses and high-pressure (HP) migmatites (Massonne et al., 2013; Cruciani et al., 2014 a,b; Fancello et al., 2018), which reached the sillimanite+K-feldspar grade (Franceschelli et al., 2005a). Within the HGMC also orthogneisses, calc-silicate nodules and metabasite lenses (basic and ultrabasic rocks with eclogite and granulite facies relics: Franceschelli et al., 2007; Cruciani et al., 2011, 2012, 2015c) occur. The L-MGMC is made up of micaschists and paragneisses (Connolly et al., 1994), with locally enclosed quartzite and metabasite bodies (Cappelli et al., 1992; Cruciani et al., 2010, 2015 a,b).

In the Inner Zone of the basement in northern Sardinia

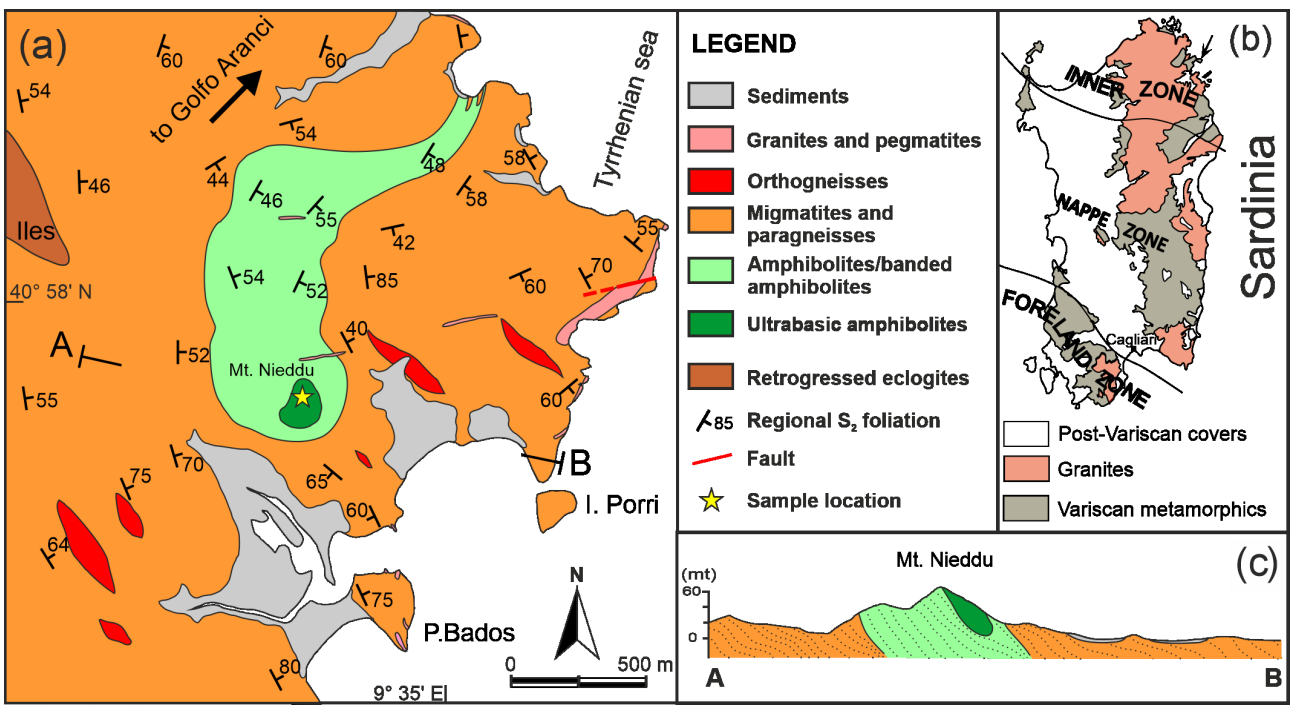

Figure 1. a) Geological sketch map of the Montigiu Nieddu area (Golfo Aranci) and location (star) of the studied samples. Modified from Scodina et al. (2019). The inset - b) shows a simplified tectonic sketch map of the Sardinian Variscan chain. Arrow shows the study area. c) Schematic section across Mt. Nieddu.

a polyphase ductile deformation was recognized and described by several authors (Carosi et al., 2005; Franceschelli et al., 2005a; Elter et al., 2010). The oldest deformation phase (D_1) is well preserved in the metamorphic rocks of the L-MGMC, especially in the Nurra-Asinara area (Cruciani et al., 2013). This deformation phase has been referred to the collisional stage (Carmignani et al., 1994) and has been dated at 345-340 Ma (Ferrara et al., 1978; Di Vincenzo et al., 2004). Within the Migmatite Complex, a D_1 deformation is documented by the transposition of centimetre-thick leucosomes, although this deformation phase is not clearly recognizable in the field.

The D_2 deformation phase is related to the development of NE-verging folds and dextral shear zones. A D_2-related shear belt is located between the L-MGMC and the HGMC (former Posada-Asinara line). In the Migmatite Complex of NE Sardinia, the D_2 phase is shown by N140°-striking isoclinal folds with a SE dip of 2-18°. Corsi and Elter (2006) documented the occurrence of two opposite senses of shear (top to NW and top to SE/NE) on the D_2-related foliation, which have been interpreted by these authors as being due to non-coaxial D_1 and D_2 deformational events. They associated the top-to-NW shear component with the end of compression and crustal thickening, whereas the top-to-SE/NE component derived from tectonic inversion during the exhumation of the metamorphic basement.

The D_3 deformation phase consists of upright metric to decametric open folds developed after D_2. Folds related to D_3 are associated with an S_3 axial-plane crenulation cleavage. The D_4 tectonic phase is revealed by metric to decametric folds with sub-horizontal axial planes.

A synoptic table, presenting deformation, metamorphic and magmatic events in the Variscan basement of Sardinia, can be found in Cruciani et al. (2015c). The metamorphic basement was finally intruded by Permo-Carboniferous granites emplacing between 340 and 280 Ma (Carmignani et al., 2001; Di Vincenzo et al., 2004 and references therein). Carboniferous-Permian sedimentary basins (Barca et al., 1995) and Permian volcanism cover part of the crystalline basement.

FIELD GEOLOGY

The study area is located in the HGMC of northeastern Sardinia. The studied rocks were sampled at Mt. Nieddu (Figures 1, 2a) a few kilometres NE of the town of Olbia, where the 0.5x1.5 km^2 lensoid amphibolite body crops out. The banded amphibolite of this body mainly consists of an alternation of dark, amphibole-rich and whitish, plagioclase-rich layers, best recognizable in the outer part of the Mt. Nieddu metabasite lens. Both layers are composed of amphibole, plagioclase, quartz, garnet, and rare clinopyroxene in variable modal proportions. No relics of magmatic minerals were found. The dark and whitish layers are parallel to the main regional schistosity S_2 which shows a prevalent NE-SW strike direction. S_2 is in turn folded by hectometre-sized F_3 folds, the axis of which strikes NW-SE. More details on the banded amphibolite can be found in Scodina et al. (2019). The contact between the ultrabasic amphibolite and the banded amphibolite is sharp and strikes N 40° and dips SE 45°. Although strongly retrogressed by the growth of large amphibole grains, the ultrabasic amphibolite preserved relics of igneous minerals (olivine, plagioclase, orthopyroxene, clinopyroxene). On the basis of the distribution of minerals and their microstructures three main compositional layers of the ultrabasic amphibolite have been distinguished (layers A, B, and C: Cruciani et al., 2002; Franceschelli et al., 2002).

The lowermost layer (layer A, Cruciani et al., 2002) is dark-grey and reddish in colour and about 20 m thick. The rocks of this layer are characterized by the occurrence of igneous olivine grains, which are locally surrounded by a discontinuous thin layer of orthopyroxene. Igneous prismatic pyroxene occurs together with amphibole, garnet, plagioclase, chlorite, and a large amount of green spinel, which forms worm-like structures and patches

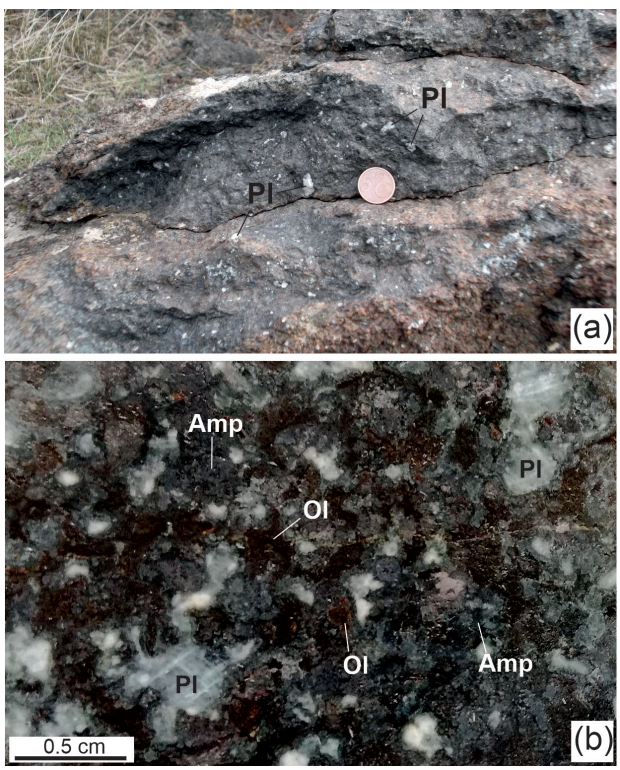

Figure 2. Field photograph (a) and cutted and polished hand specimen (b) of layer B of the ultrabasic amphibolite from Mt. Nieddu. Pl=plagioclase; Ol=olivine; Amp=amphibole.

either in association with amphibole or around garnet. Chlorite often occurs in small veins which can additionally contain late-stage amphibole.

The middle layer B is around 5 m thick, lenticular, dark grey to greenish in colour. The rock consists mainly of greenish amphibole and large igneous olivine and plagioclase crystals (up to 1 cm, Figure 2 a,b). Its microstructural features will be described in detail in the next chapters.

The uppermost layer C (15-20 m in thickness) is dark-green and rich in garnet. The rocks of this layer, which occurs at the top of Mt. Nieddu, are characterized by the presence of porphyroblastic garnet and large amphibole grains (up to 4-5 cm). Also spinel, plagioclase, pyroxene, and chlorite can be found within this layer. Layer C is featured by the occurrence of garnet-rich nodules, ranging in size from 1 to 15 cm, and garnet- and/or amphibole-rich veins. The nodules, which are made up of coarse-grained garnet, amphibole, spinel, and abundant epidote, are often surrounded by a 1-2 mm thick amphibole-rich rim or crosscut by amphibole-rich veins. Garnet occurs as anhedral crystals with inclusions of epidote and green amphibole.

The migmatites, hosting the large lensoid amphibolite body, are coarse-grained with stromatic fabric, show a well-developed S_2 foliation, and were derived from an original psammitic to pelitic sequence. More details on the adjacent migmatite structure and mineralogy can be found in Massonne et al. (2013) and Cruciani et al. (2014a). All metamorphic rock types in the study area are crosscut by metre-sized dykes of leucogranitic composition.

ANALYTICAL METHODS

Microstuctural studies of selected samples of the ultrabasic amphibolite in layer B from Mt. Nieddu were made with a FEI Quanta 200 scanning electron microscope equipped with a Thermo Fisher energy-dispersive microanalysis system at Centro Servizi di Ateneo per la Ricerca (CeSAR), Università di Cagliari. For these studies, carbon-coated polished thin-sections were previously prepared. Mineral modes were determined by image-analysis with the computer software ImageJ.

The chemical compositions of the main rock-forming minerals were determined with a CAMECA SX100 electron microprobe (EMP) equipped with five wave-length dispersive (WD) spectrometers at the Institut für Mineralogie und Kristallchemie, Universität Stuttgart. The operative conditions for a ca. two-minutes-lasting full analysis included 15 kV acceleration voltage, 15 (garnet) or 10 nA (other silicates, ilmenite) beam current, and a 5 μm spot size. For the description of the used standards, counting times and analytical errors see Massonne (2012). Structural formulae were calculated on the basis of 12, 6, 8, 4, 28, 12.5 oxygen anions for garnet, pyroxene, plagioclase, spinel, chlorite, and epidote, respectively. The amphibole structural formula was calculated for 23 oxygen anions using the CalcMin program (Brandelik, 2009).

PETROLOGICAL INVESTIGATION

Petrography

For this study, samples MNX and MNY (for locations see Figure 1) have been selected from layer B of the ultrabasic amphibolite from Mt. Nieddu. Sample MNX (Figures 2b, 3 a,b,c) is made up of amphibole (20 vol%), olivine (18 vol%), orthopyroxene (15 vol%), garnet (15 vol%), plagioclase (12 vol%), clinopyroxene (10 vol%), spinel (7 vol%), epidote (2 vol%), chlorite (1 vol%), and corundum (<1 vol%). Sample MNY (Figure 3d) consists of olivine (21 vol%), amphibole (21 vol%), orthopyroxene (12 vol%), garnet (17 vol%), plagioclase (11 vol%), spinel (5 vol%), clinopyroxene (7 vol%), epidote (2 vol%), chlorite (1 vol%), and corundum (<1 vol%).

Even if strongly retrogressed by the growth of large amphibole grains and other late phases, these samples preserve relics of igneous minerals (olivine Ol_0, plagioclase Pl_0, orthopyroxene Opx_0, clinopyroxene Cpx_0, Figures 3 a,b,c, 4 a,b). Opx_0 is featured by the occurrence of thin oriented trails of Fe-oxides in the core of the crystals. Cpx_0 is partially replaced by brown and green amphibole. The most striking feature of these rocks is the occurrence of multilayer corona textures around Ol_0 and Pl_0 relics.

Ol_0 is anhedral and millimetric in size (1-5 mm). It is intensely fractured and altered along the cracks which are filled with Ca-amphibole (Amp_{2a-b}), talc, serpentine and Fe-oxides. Talc appears to be more abundant than serpentine at the margin of the igneous mineral. Ol_0 is surrounded by a sub-millimetric rim of Opx_1 which, in turn, is frequently surrounded by a thinner discontinuous rim of clinopyroxene (Cpx_{1a}) (Figures 3b, 4b). A Fe-Mg-amphibole (Amp_{2c}) can locally overgrow Opx_1. Amp_{2c} and talc can be found also inside Opx_1 fractures.

Pl_0 is anhedral and partially replaced by mostly clinozoisite-epidote, which can be zoned featuring an earlier Fe-bearing (Ep_{3a}) and a later Fe-free variety (Ep_{3b}, Figures 3c, 4 a,d), and chlorite. The latter phase also shows two varieties, which can be distinguished by different Mg and Fe contents: earlier Chl_2 has higher Mg and lower Fe contents compared to later Chl_3. Pl_0 (and phases that have replaced it) is surrounded by a discontinuous symplectite-type microstructure of spinel and clinopyroxene (Cpx_{1b}+Spl_1) (Figures 3d, 4e). Locally, submillimetric spinel crystals are clustered to form a thin layer around Pl_0. A garnet corona (Grt_1) with variable sub-millimetric thickness (Figures 3 b,d, 4 a,b,c,d,f) is in turn found around the above mentioned

symplectite. Grt_1 shows abundant cracks, which are filled with Chl_3, and inclusions of Cpx_{1b}+Spl_1 symplectite, as well as elongated to rounded inclusions of Spl_1 (Figure 4 b,d,f). Corundum (Crn_2) has partially replaced Spl_1 of the symplectite (Figure 4 d,f), but is not always present in the coronae. Outside the garnet layer, at the contact with amphibole, a very thin rim of spinel (Spl_2) can occur. Spl_2 grew as vermicular symplectitic microstructure together with Amp_{2a-b} in the interface between Grt_1 and amphibole of the matrix (Amp_{2a-b}) (Figure 3d). Between Ol_0 and Pl_0 and their coronae, green amphibole (Amp_{2a}) and minor brown amphibole (Amp_{2b}) grew to variable extent. Amp_{2b} generally formed around igneous relics of Cpx_0 (Figure 3a) as well. The above described amphiboles can be locally replaced by a late actinolite (Amp_3) growing at their margins.

The aforementioned coronitic textures are characterized also by a minor but widespread occurrence of small ilmenite in contact with magnetite. Other accessory minerals found in these rocks are calcite, dolomite, apatite, and Zn-sulphide.

On the basis of petrological and microtextural features of the studied samples, it is possible to distinguish four stages of mineral formation (Figure 5): (1) an igneous stage, documented by the relics of igneous minerals which can be easily distinguished by their medium-grain size and habitus from later minerals, (2) a first stage of metamorphic re-equilibration, documented by the formation of coronitic (Opx_1, Cpx_{1a}, Grt_1) and symplectitic (Spl_1+Cpx_{1b}) minerals, (3) a second stage of metamorphic

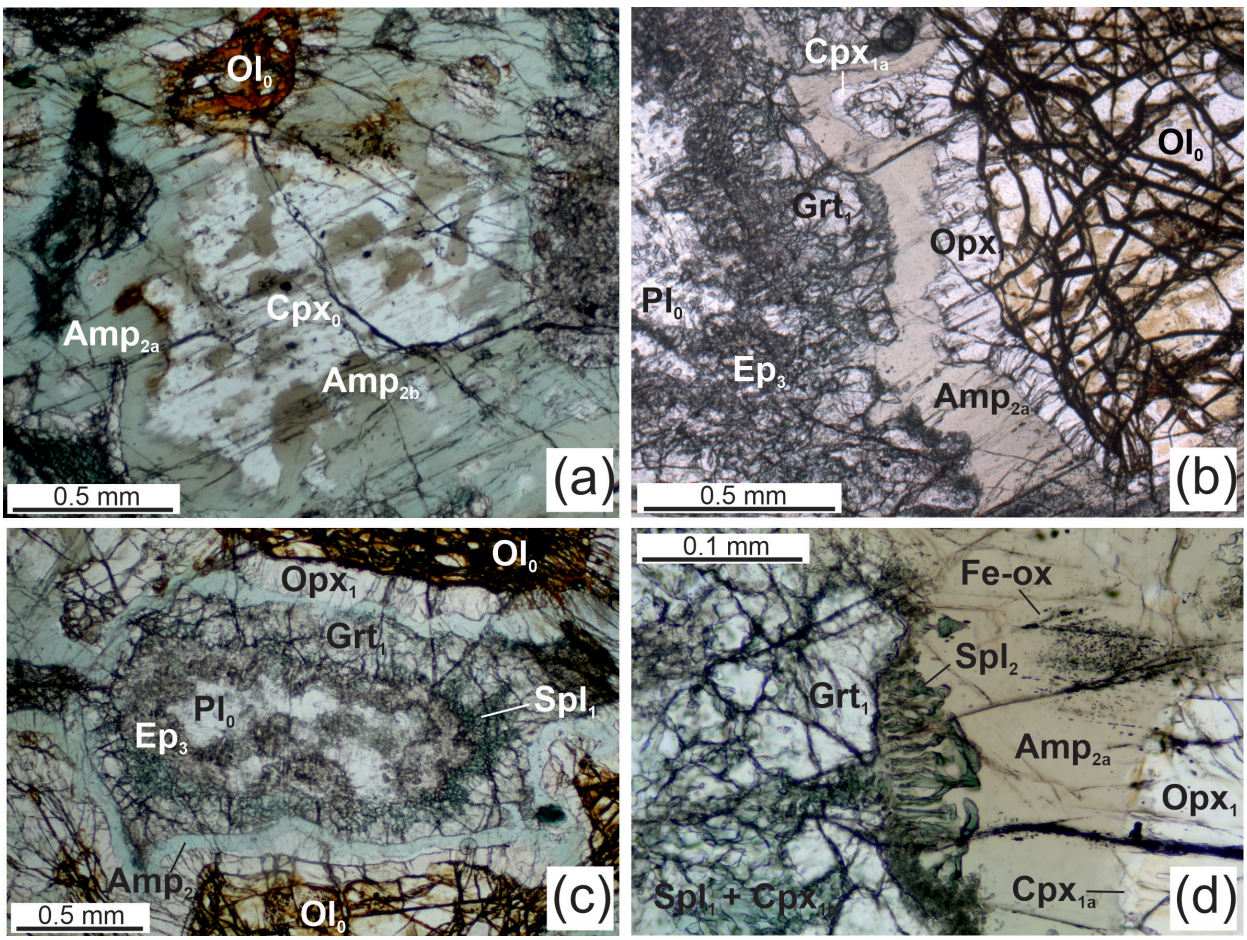

Figure 3. Photomicrographs under plain polarized light showing the relevant microstructures of rocks from layer B in the ultrabasic amphibolite from Mt. Nieddu. a) Detail of an igneous clinopyroxene overgrown by green and brown amphibole, sample MNX; b) Sequence of coronitic minerals from igneous plagioclase (left) to olivine (right); sample MNX. c) Overview of coronitic textures with an igneous plagioclase relic in the centre, sample MNX; d) Detailed view of the vermicular microtextures of spinel, at the interface between garnet and amphibole, sample MNY; Pl=plagioclase; Ol=olivine; Grt=garnet; Opx=orthopyroxene; Cpx=clinopyroxene; Amp=amphibole; Spl=spinel.

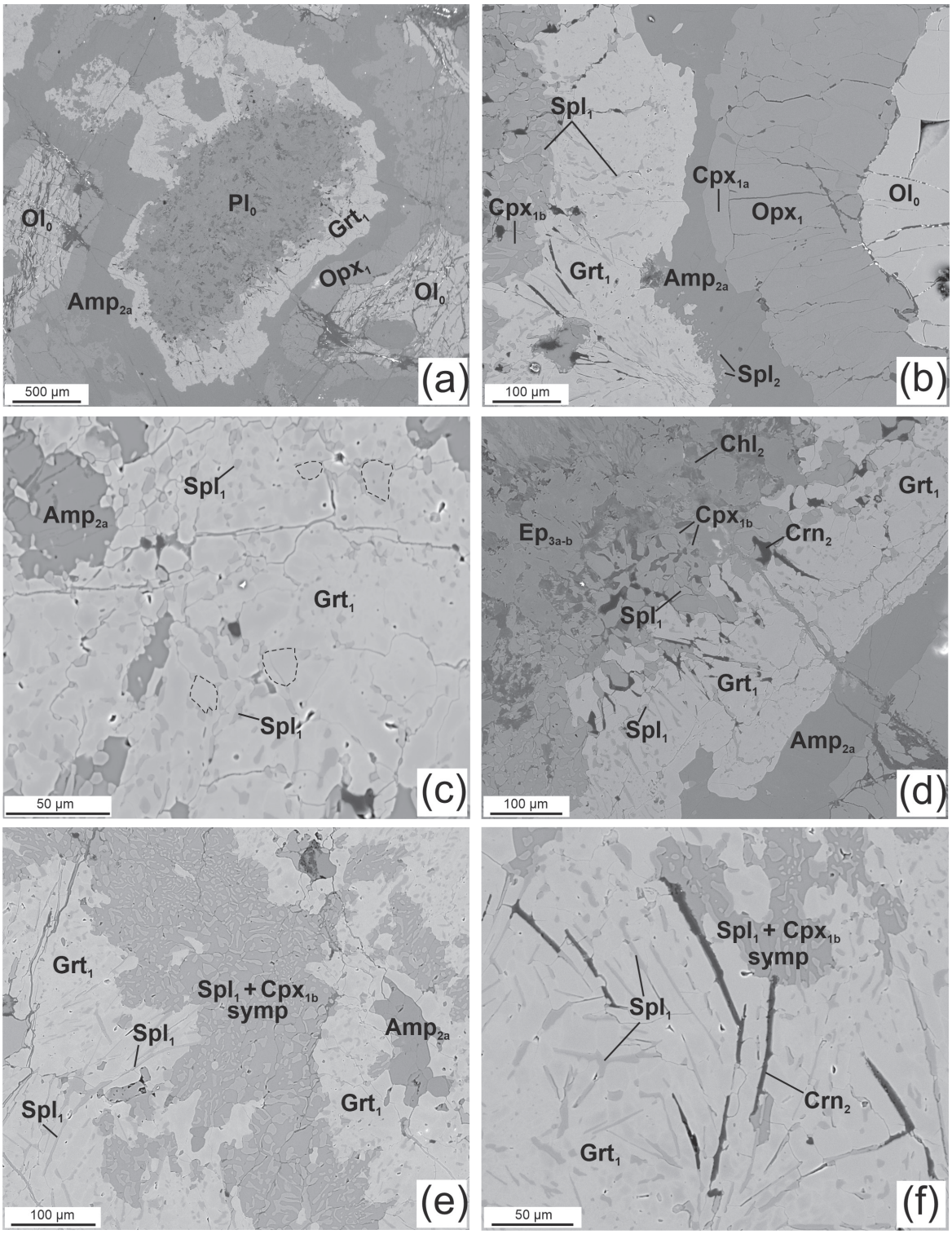

Figure 4. BSE images showing the relevant microstructures of rocks from layer B in the ultrabasic amphibolite from Mt. Nieddu. a) Overview of coronitic textures around an igneous plagioclase relic, sample MNX; b) Detailed view of the sequence of coronitic minerals, sample MNY; c) Patchy zoning in garnet; a few patches have been contoured, sample MNY; d) Inclusions in coronitic garnet, sample MNX; e) Symplectite of spinel and clinopyroxene associated with garnet, sample MNX; f) Corundum replacing spinel at the interface between symplectite and garnet, sample MNX; Mineral abbreviations as in Figure 3. Crn=corundum; Ep=epidote; Chl=chlorite.

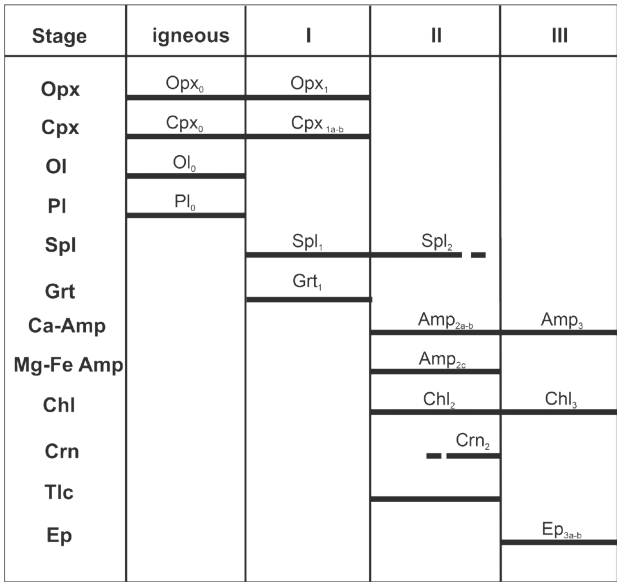

Figure 5. Metamorphic and mineralogical evolution scheme of coronitic textures of rocks from layer B in the ultrabasic amphibolites from Mt. Nieddu. Mineral abbreviations as in Figure 4. Stage I: formation of coronitic and symplectitic minerals; Stage II: growth of amphibole and spinel; Stage III: late re-equilibration.

re-equilibration, represented by the massive overgrowth of brown and green amphibole (Amp_{2a-b}) and the formation of spinel (Spl_2) over the coronitic assemblages (other minerals attributed to this stage are Chl_2, talc, and Crn_2), and (4) a third metamorphic stage documented by the local growth of late phases such as actinolite (Amp_3), chlorite (Chl_3), and epidote ($Ep_{3a, 3b}$) which overgrew or replaced minerals of the previous stages.

Mineral chemistry

Representative EMP analyses of olivine, plagioclase, pyroxene, garnet, amphibole, spinel, chlorite, and epidote from samples MNX and MNY are reported in tabs. 1 to 4. Ol_0 is homogeneous in composition with X_{Mg}=Mg/(Mg+Fe^{2+}) ranging from 0.69 to 0.71. Pl_0 is anorthite with X_{Ca}=Ca/(Na+Ca) values in the range 0.95-0.98. Opx_0 and Opx_1 are bronzites with X_{Mg} of 0.76-0.77. Opx_1 is compositionally homogeneous across the coronitic layer. Al_{tot} contents of Opx_1 are around 0.04 atoms per formula unit (apfu). Calculated Fe^{3+} contents are between 0.03 and 0.05 apfu.

Cpx_0 is diopside with X_{Mg} around 0.84. Cpx_{1a} is also diopside with X_{Mg} between 0.88 and 0.92. A higher X_{Mg} of 0.93-0.94 was observed for Cpx_{1b} associated with Spl_1. In addition, Cpx_{1b} is characterized by an Al_{tot} content higher than that of Cpx_0 and Cpx_{1a} (around 0.26 apfu versus 0.03-0.06 apfu of $Cpx_{0\text{-}1a}$). Grt_1 contains 37-39 mol % almandine, ~1 mol % spessartine, and intermediate pyrope and grossular contents of 30-32 mol % and 27-31 mol %, respectively. Careful observations by SEM of Grt_1 reveals a very slight patchy zoning (Figure 4c) in which, however, most compositional differences are within the analytical error.

With the exception of Amp_{2c}, amphibole is calcic according to the classification of Leake at al. (1997). Brown amphibole (Amp_{2b}) ranges in composition from Mg-hornblende to edenite with Si=6.5-6.6 apfu and X_{Mg} values from 0.84 to 0.94. The Na content is variable from 0.40 to 0.65 apfu. Green amphibole (Amp_{2a}) is pargasite with Si=6.1-6.3 apfu and X_{Mg} values between 0.77 and 0.90. Amp_{2c} is a Mg-Fe amphibole with Si and X_{Mg} around 7.9 apfu and 0.77, respectively. Amp_3 is actinolite with Si=7.6-7.7 apfu and X_{Mg} between 0.83 and 0.87.

Spl_1 and Spl_2 belong to the spinel s.s.-hercynite solid-solution series with low Cr content (~0.01 wt% Cr_2O_3). X_{Mg} values of Spl_1 are around 0.55 whereas Spl_2 shows lower X_{Mg} values (0.45-0.46) and consequently higher FeO contents (22-24 wt%). Chl_2 is clinochlore with Si=5.4-5.7 apfu and an Fe content between 1.6 and 2.0 apfu. X_{Mg} values vary between 0.70 and 0.75. Chl_3 is ripidolite with Si=5.4-5.5 apfu and an Fe content between 4.7 and 4.9 apfu. X_{Mg} values are around 0.45. Talc shows Fe contents up to 0.40 apfu. Epidote is zoned from Ep_{3a} with Fe^{3+} up to 0.30 apfu to Ep_{3b} with Fe^{3+}<0.05 apfu. Ilmenite grains associated with magnetite have variable MnO and MgO contents between 0.7 and 2.6 wt% and 0.9 and 1.8 wt%, respectively. Magnetite shows TiO_2 contents between 2 and 6 wt% and Al_2O_3 contents around 1.5 wt%.

MODELLING OF CORONA REACTIONS

In order to verify the sequence of the corona reactions on the basis of the microstructural observations, petrological data have been merged with quantitative balancing of metamorphic reactions by the "least-squares" method using the CSPACE software (Torres-Roldan et al., 2000). Using the composition of the main phases in the MNX and MNY samples (Tables 1-4) in terms of apfu as input data, this software calculates the possible reactions between the phases used as input data. A proper resulting reaction should be coherent with the observed microstructures (i.e. the reactants and products should appear on opposite sides of the modelled reaction) and the stoichiometric coefficients should be in agreement with the observed amounts of mineral products.

Formation of coronae and symplectites

As stated by Korzhinskii (1959) and Thompson (1959), who provided the foundation concerning mass transfer in metamorphic rocks, and more recently by Gaidies et al. (2017), the formation of a series of sharply-bounded

Table 1. Representative electron microprobe analyses (wt%) of igneous olivine and plagioclase and coronitic garnet from samples MNX and MNY.

	MNX		MNY	MNX		MNY	MNX	MNY	
	Ol_0	Ol_0	Ol_0	Pl_0	Pl_0	Pl_0	Grt_1	Grt_1	Grt_1
SiO_2	37.24	37.60	37.63	43.24	42.96	42.60	39.90	39.68	38.94
TiO_2	-	0.01	0.01	0.01	-	0.02	0.03	-	0.02
Al_2O_3	-	-	-	35.43	35.07	35.11	22.45	22.44	22.10
FeO	26.77	27.05	27.40	0.38	0.04	0.04	19.32	18.84	18.08
MnO	0.20	0.22	0.23	-	0.05	0.02	0.61	0.69	0.68
MgO	36.06	36.06	36.29	-	-	-	8.90	8.36	8.27
CaO	0.03	-	0.00	19.81	20.29	20.12	10.43	11.25	11.87
Na_2O	-	-	-	0.25	0.16	0.12	-	-	-
K_2O	-	-	-	0.03	0.01	0.01	-	-	-
Total	100.30	100.94	101.56	99.15	98.58	98.04	101.64	101.26	99.96
Oxygen	4	4	4	8	8	8	12	12	12
Si	0.98	0.99	0.99	2.02	2.02	2.02	2.98	2.98	2.96
Ti	-	0.00	-	0.00	-	0.00	0.00	-	0.00
Al	-	-	-	1.96	1.95	1.96	1.98	1.99	1.98
Fe^{2+}	0.59	0.59	0.60	-	-	-	1.21	1.18	1.15
Fe^{3+}	-	-	-	0.02	0.00	0.00	-	-	-
Mn	0.00	0.00	0.01	-	0.00	0.00	0.04	0.04	0.04
Mg	1.42	1.41	1.42	-	-	-	0.99	0.94	0.94
Ca	0.00	-	0.00	0.99	1.02	1.02	0.84	0.91	0.97
Na	-	-	-	0.02	0.02	0.01	-	-	-
K	-	-	-	0.00	0.00	0.00	-	-	-
Total	2.99	2.99	3.02	5.01	5.01	5.01	8.04	8.04	8.04
X_{Mg}	0.71	0.70	0.70	-	-	-	0.45	0.44	0.45
X_{Ca}	-	-	-	0.98	0.99	0.99	-	-	-
Alm	-	-	-	-	-	-	0.40	0.38	0.38
Prp	-	-	-	-	-	-	0.32	0.31	0.30
Grs	-	-	-	-	-	-	0.27	0.30	0.31
Sps	-	-	-	-	-	-	0.01	0.01	0.01

-: below detection limit.

coronitic mineral layers is produced by chemical mass transport along chemical potential gradients which are driven by the unstable coexistence of mineral phases (here: Ol_0 and Pl_0).

The earliest metamorphic event recognizable in the studied rocks is represented by the reactions of igneous Ol_0 and Pl_0 to form Opx_1, Cpx_{1a}, Cpx_{1b}+Spl_1 (symplectite) corona and Grt_1 (Figure 6 a,b,c). On the basis of petrographic observations, the corona formation around olivine and plagioclase can be modelled in two steps that

Table 2. Representative electron microprobe analyses (wt%) of different textural varieties of pyroxene from samples MNX and MNY.

	MNX			MNY			
	Opx_0	Opx_1	Cpx_{1a}	Cpx_0	Opx_1	Cpx_{1a}	Cpx_{1b}
SiO_2	54.83	54.55	53.73	54.38	54.70	53.92	50.06
TiO_2	0.02	0.00	0.01	0.27	-	0.03	0.04
Al_2O_3	0.95	0.96	1.11	1.30	0.86	0.78	6.32
FeO	16.37	16.25	4.68	5.24	16.83	4.69	5.33
MnO	0.14	0.26	0.01	0.06	0.20	0.11	0.05
MgO	28.18	27.71	16.40	15.50	27.74	16.39	15.22
CaO	0.30	0.32	24.84	23.45	0.30	24.22	23.89
Na_2O	-	-	0.15	0.11	-	0.14	0.11
Total	100.79	100.05	100.93	100.31	100.63	100.28	101.02
Oxygen	6	6	6	6	6	6	6
Si	1.96	1.96	1.95	1.98	1.96	1.97	1.81
Ti	0.00	0.00	0.00	0.01	-	0.00	0.00
Al	0.04	0.04	0.05	0.06	0.04	0.03	0.26
Fe^{3+}	0.05	0.03	0.07	0.00	0.04	0.04	0.11
Fe^{2+}	0.44	0.46	0.08	0.16	0.46	0.11	0.05
Mn	0.00	0.01	0.00	0.00	0.01	0.00	0.00
Mg	1.50	1.49	0.89	0.84	1.48	0.89	0.82
Ca	0.01	0.01	0.97	0.92	0.01	0.95	0.93
Na	-	-	0.01	0.01	-	0.01	0.01
Total	4.00	4.00	4.02	3.98	4.00	4.00	3.99
X_{Mg}	0.77	0.77	0.92	0.84	0.76	0.89	0.94

are part of the schematic single reaction Pl+Ol=Opx+Cpx+Spl+Grt: (i) formation of $Cpx_{1a,b}$, Opx_1, Spl_1 and (ii) subsequent formation of Grt_1. Corresponding reaction 1, modelled for sample MNX with CSpace is:

$$0.36Pl_0+0.70Ol_0=0.34Opx_1+0.37Cpx_{1a}(\text{or } Cpx_{1b})+0.35Spl_1 \quad (1)$$

The calculated reaction is compatible with the observations on the samples (section 5.1, Figure 6b). The reliability of the reaction is also supported by the relative volumes of the reactants and products calculated from the stoichiometric coefficients and the molar volumes available from the literature (Helgeson et al., 1978) and reported in Table S1 of Supplementary Information. These coefficients are compatible with the observed modal contents (cf. section Petrography) of the minerals with the exception of clinopyroxene. The predicted modal content of this mineral is overestimated probably due to its involvement and consumption in subsequent reactions. The above reconstructed reaction 1 likely represents a partially stable state of reaction progress dominated by the breakdown of the igneous phases Ol_0 and Pl_0.

Considering that Grt_1 contains inclusions of Spl_1 and $Cpx_{1b}+Spl_1$ symplectite (Figure 4 b,d,e,f), the growth of Grt_1 is likely controlled by reaction 2 (Figure 6c):

$$0.69Cpx_{1a\text{-}b}+0.52Spl_1=0.51Grt_1 \quad (2)$$

In this case, due to the few phases involved in the modelled reaction, the calculated residuals are higher than for reaction 1, especially related to MgO.

Table 3. Representative electron microprobe analyses (wt%) of different textural varieties of amphibole from samples MNX and MNY. The H_2O content was calculated.

	MNX		MNY		
	Amp_{2b}	Amp_{2a}	Amp_{2a}	Amp_{2c}	Amp_3
SiO_2	46.04	44.92	45.16	57.10	55.34
TiO_2	0.51	0.05	0.07	-	0.57
Al_2O_3	12.46	13.83	13.54	0.50	1.95
FeO	5.48	3.35	2.96	13.80	5.20
Fe_2O_3	2.54	5.16	5.18	-	0.27
MnO	0.05	0.03	0.05	0.20	0.18
MgO	16.08	16.09	16.23	25.40	20.47
CaO	12.56	12.54	12.32	-	11.76
Na_2O	2.28	2.27	2.26	-	1.79
K_2O	0.13	0.08	0.11	-	0.63
H_2O	2.11	2.12	2.12	2.14	2.15
Total	100.24	100.45	100.00	99.14	100.31
Oxygen	23	23	23	23	23
Si	6.53	6.35	6.39	7.98	7.71
Al^{IV}	1.47	1.65	1.60	0.02	0.29
Al^{VI}	0.62	0.65	0.66	0.07	0.03
Ti	0.05	0.01	0.01	-	0.06
Fe^{2+}	0.65	0.40	0.35	1.61	0.61
Fe^{3+}	0.27	0.55	0.55	-	0.03
Mn	0.01	0.00	0.01	0.02	0.02
Mg	3.40	3.39	3.43	5.29	4.25
Ca	1.91	1.90	1.87	-	1.76
Na	0.63	0.62	0.62	-	0.48
K	0.02	0.01	0.02	-	0.11
H	2.00	2.00	2.00	2.00	2.00
Total	17.56	17.53	17.51	16.99	17.35
X_{Mg}	0.84	0.89	0.90	0.77	0.87
	edenite	pargasite	pargasite	cum.	actinolite

Destabilization of the coronae

The subsequent reaction 3, occurring in the studied rocks during the second metamorphic stage of re-equilibration, led to the consumption of the coronae due to the formation of green and brown amphibole (Amp_{2a} and Amp_{2b}) and spinel (Spl_2) (Figure 6d):

$$0.89Spl_1+0.04Opx_1+0.07Grt_1+0.02Cpx_{1a}+0.05H_2O=0.05Amp_{2a}+0.45Spl_2 \quad (3)$$

The various amphiboles overgrew the relics of the igneous pyroxenes (Cpx_0, Opx_0) and grew within the corona structures that had developed between Ol_0 and Pl_0.

Table 4. Representative electron microprobe analyses (wt%) of different textural varieties of spinel, chlorite, and epidote from samples MNX and MNY. The H_2O content was calculated for chlorite and epidote.

	MNX	MNY			MNX	MNY			MNX	MNY
	Spl_1	Spl_1	Spl_2		Chl_2	Chl_2	Chl_3		Ep_{3a}	Ep_{3b}
SiO_2	-	0.04	0.05	SiO_2	29.45	29.21	25.71	SiO_2	39.10	39.50
TiO_2	-	0.01	0.02	TiO_2	-	-	-	TiO_2	0.01	0.01
Al_2O_3	63.42	62.63	59.38	Al_2O_3	27.94	28.08	19.98	Al_2O_3	31.77	33.77
Cr_2O_3	0.01	-	0.03	FeO	11.03	11.00	27.38	Cr_2O_3	-	-
FeO	20.56	20.21	22.86	MnO	0.10	0.09	0.99	Fe_2O_3	3.09	0.22
Fe_2O_3	1.86	2.37	4.63	MgO	17.52	17.67	13.94	FeO	-	-
MnO	0.05	0.09	0.17	H_2O	12.31	12.31	11.24	MnO	-	-
MgO	13.90	13.95	11.81	Total	98.35	98.36	99.24	MgO	-	-
CaO	0.11	0.10	0.01	Oxygen	28	28	28	CaO	24.52	24.94
Total	99.91	99.40	98.96	Si	5.38	5.69	5.48	H_2O	1.97	1.99
Oxygen	4	4	4	Al	2.26	2.31	5.02	Total	100.46	100.43
Si	-	0.00	0.00	Ti	-	-	-	Oxygen	12.5	12.5
Al	1.96	1.95	1.90	Fe^{2+}	1.80	1.79	4.88	Si	2.98	2.98
Ti	-	0.00	0.00	Mn	0.02	0.01	0.18	Al	2.85	3.00
Fe^{2+}	0.45	0.45	0.52	Mg	5.09	5.13	4.43	Ti	0.00	0.00
Fe^{3+}	0.04	0.05	0.09	H	16.00	16.00	16.00	Fe^{2+}	-	-
Cr	0.00	-	0.00	Total	30.55	31.04	35.99	Fe^{3+}	0.18	0.01
Mn	0.00	0.00	0.00	X_{Mg}	0.74	0.74	0.47	Cr	-	-
Mg	0.54	0.55	0.48					Mn	-	-
Ca	0.00	0.00	0.00					Mg	-	-
Total	2.99	3.00	2.99					Ca	2.00	2.02
X_{Mg}	0.55	0.55	0.45					Total	8.01	8.01

Spl_2 grew as vermicular symplectitic microstructure at the interface between Grt_1 and Amp_{2a}. The calculated reaction 3 is compatible with the observations on the samples in regard to the coronitic phases as reactants and Amp_{2a} and Spl_2 as products (Table S1). Although the content of spinel in the rock seems to be lower than that reported in Table S1, in the microdomain, in which amphibole and spinel are associated (Figure 3d), the observed modal content of spinel is comparable to the calculated one.

GEOTHERMOBAROMETRY

The study of coronitic assemblages of the rocks in layer B allows us to constrain the P-T conditions of the corona formation applying conventional geothermobarometry and modelling with P-T pseudosections.

Conventional thermobarometry

Chemical compositions of coronitic minerals used for the application of conventional thermobarometry were taken in close proximity to each other (as suggested by Jašarová et al., 2016), because during formation of corona layers equilibrium was reached only locally, at least at grain contacts (Gaidies et al., 2017). We estimated the P-T conditions of the crystallization of the igneous protolith applying the geothermometer that is based on the distribution of $Mg_2Si_2O_6$ between orthopyroxene and clinopyroxene (two-pyroxene thermometer). The application of this geothermometer on Opx_0 and Cpx_0 relics yielded temperatures of 773-780 °C with the calibration of Brey and Köhler (1990) and 832-843 °C using the calibration of Putirka (2008) for the pressure interval of 0.2

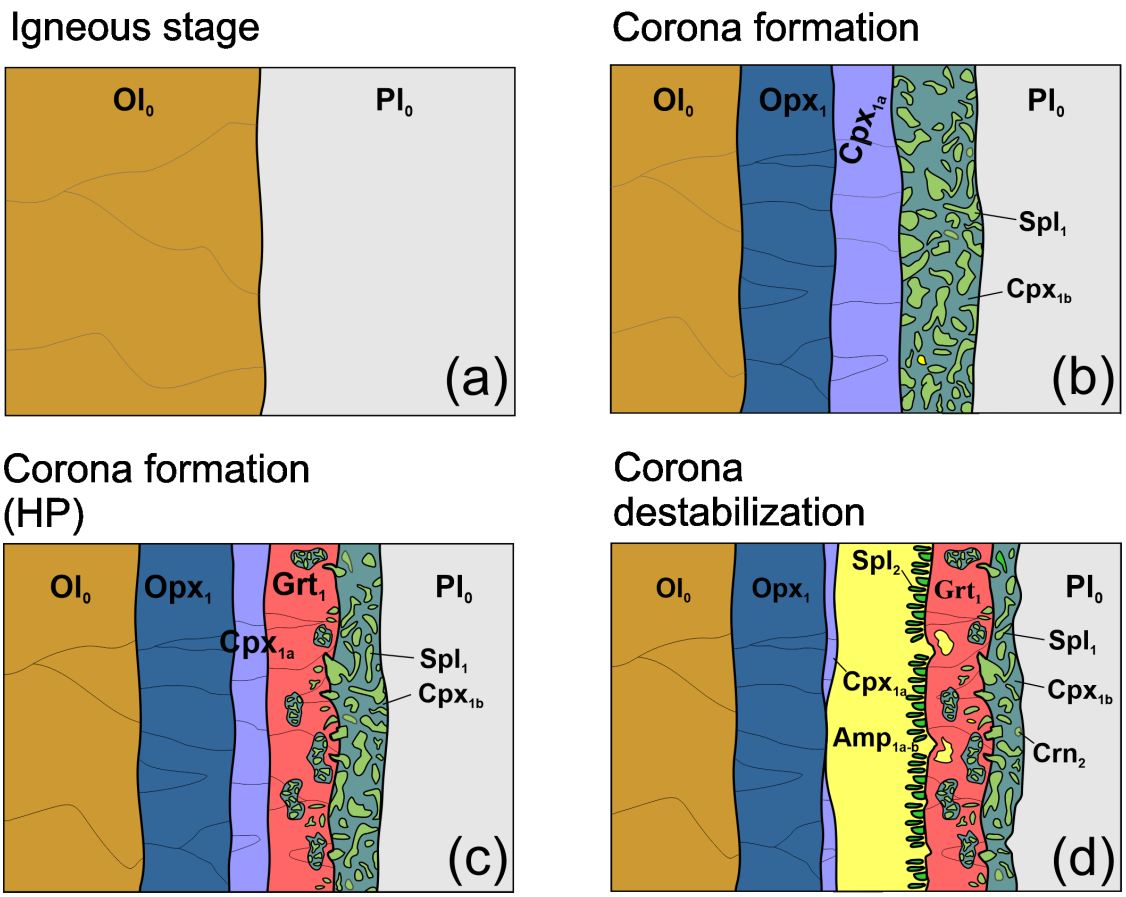

Figure 6. Metamorphic evolution of coronitic microstructures of rocks from layer B in ultrabasic amphibolites from Mt. Nieddu. Mineral abbreviations as in Figure 4.

to 0.6 GPa. Temperatures <800 °C seem to be too low with respect to the solidus of gabbroic rocks. The similarity to Cpx_1-Opx_1 temperatures (up to 790 °C) may suggest a low-temperature re-equilibration of the igneous minerals. The magmatic assemblage of orthopyroxene, clinopyroxene, Mg-rich olivine, and plagioclase suggests that magmatic crystallization occurred at pressures lower than 0.8 GPa for temperatures around 840 °C (Putirka, 2008).

The temperature condition of formation of corona garnet (i.e. granulite-stage temperatures) was determined with the garnet-clinopyroxene and clinopyroxene-orthopyroxene geothermometers based on exchange of Mg and Fe^{2+} between the corresponding phases. The chemical compositions of Grt_1 and Cpx_{1a} used for the calculations were taken from the same corona domain. For each sample at least three corona domains were analyzed. Estimated temperatures with the garnet-clinopyroxene thermometer, using the calibrations of Powell (1985) and Ellis and Green (1979), range between 650 and 720 °C. Temperatures calculated with the two-pyroxene thermometer applied to coronitic pyroxenes (Cpx_{1a} and Opx_1) are between 630 and 790 °C using the calibration of Brey and Köhler (1990). Temperature values related to the destabilization of corona garnet (amphibolite stage) were obtained by the magnetite-ilmenite thermometer using the calibrations of Stormer (1983), Lindsley and Spencer (1982), and Anderson (1968). This geothermometer, applied to ten magnetite-ilmenite couples of small crystals in mutual contact within the rock matrix, yielded temperatures between 500 and 560 °C. Similar P-T conditions for the amphibolite stage were reported by Scodina et al. (2019) for the adjacent amphibolite at Mt. Nieddu and also for several metabasites from NE Sardinia (at pressures of about 0.4-0.8 GPa) (Franceschelli et al., 2002, 2007). Unfortunately, the mineral assemblage of coronitic layers does not allow us to apply a geobarometer to determine the pressure conditions of the HP granulite stage.

P-T Pseudosections

We have used a P-T pseudosection approach to estimate the P-T conditions of corona formation with the main aim of testing this approach if it can be applied to corona

microdomains. For this purpose, we compare the results with those obtained in adjacent rocks by Scodina et al. (2019).

The mineralogical inhomogeneities in the selected samples by coronitic textures in the ultrabasic amphibolite complicate the application of the P-T pseudosection approach, because the fundamental principle of the geothermobarometry with P-T pseudosections requires equilibration within a specific sample volume (Powell and Holland, 2008). However, despite the corona textures which are usually believed to indicate a state of disequilibrium, several studies have demonstrated that equilibrium conditions may be reached at least at a microdomain scale (Bethume and Davidson, 1997 and references therein). In addition, P-T pseudosection modelling was successfully applied by several authors to coronitic assemblages to derive P-T conditions (e.g., Doukkari et al., 2015; Groppo et al., 2015).

We calculated P-T pseudosections for samples MNX and MNY in the CaO-FeO-MgO-Al_2O_3-SiO_2-H_2O (CFMASH) system using the software PERPLE_X (Connolly, 1990, 2009) and the thermodynamic data set of Holland and Powell (1998) for H_2O and minerals. The effective compositions of the corona domains used to calculate P-T pseudosections (Table 5) were obtained by the corona mineral compositions of samples MNX and MNY and the stoichiometric coefficients, calculated with the CSpace software, of the balanced reaction:

$$0.42Pl_0+0.70Ol_0=0.32Spl_1+0.37Cpx_{1a}+0.28Opx_1+0.09Grt_1 \quad (4)$$

that involves all mineral phases found in the coronitic microdomains (see Groppo et al., 2007, for method description). These compositions were then compared with the average of ten SEM-EDS areal scan analyses on 1×1 mm^2 microareas. In spite of uncertainties on the corona boundary, the area scan analyses resulted in maximum differences less than 2 wt% for SiO_2 and Al_2O_3 and even lower for all other elements as compared to the composition obtained from reaction (4).

Solid-solution models used are those of Holland and Powell (1998: garnet, white mica, spinel and olivine), Holland and Powell (1996: orthopyroxene), Green et al. (2007: clinopyroxene), Holland et al. (1998: chlorite), Powell and Holland (1999: biotite, potassic white mica), Dale et al. (2005: amphibole), and Newton et al. (1981: plagioclase). In addition, an ideal mixing model for talc was applied. All P-T pseudosections were calculated considering H_2O as a saturated phase and Fe being only divalent, because the Fe^{3+} content of the minerals in the coronitic domains is supposed to be negligible. P-T pseudosections for MNX and MNY microdomains were calculated also with different H_2O contents (5, 2, 1 wt%). Low contents led to the destabilization of hydrous minerals (amphibole, zoisite) and the appearance of olivine and orthopyroxene in the low-temperature part

Table 5. Bulk-rock composition of samples MNX and MNY determined with X-ray fluorescence spectrometry and effective compositions of corona domains used for thermodynamic calculations with PERPLE_X.

	MNX	MNX	MNY	MNY
	Bulk XRF	Effective c.	Bulk XRF	Effective c.
SiO_2	42.24	40.57	42.02	40.43
TiO_2	0.10	-	0.08	-
Al_2O_3	9.54	19.00	10.34	18.20
Fe_2O_3	17.55	-	16.95	-
FeO_{tot}	-	12.47	-	13.27
MnO	0.25	-	0.20	-
MgO	21.94	18.51	18.23	17.62
CaO	7.03	10.95	8.87	10.42
Na_2O	0.57	-	0.60	-
K_2O	0.04	-	0.04	-
P_2O_5	0.02	-	0.02	-

of the P-T diagram (i.e. <700°C). The topology of the multivariant fields at T >750°C, which are relevant for the determination of P-T conditions of our samples, remains mostly unchanged. The garnet field in the corresponding pseudosection is located at pressures >0.8 GPa for temperatures above 650 °C, whereas the plagioclase field occurs below 0.5 GPa.

In order to define the P-T conditions of the garnet formation, the calculated pseudosections were contoured by selected isopleths (Figure 7b, Figure S1 of Supplementary Information) representative of almandine, grossular, and pyrope contents in Grt_1. The intersections of the corresponding isopleths (X_{Fe}=0.39, X_{Ca}=0.27, X_{Mg}=0.31) occur around 700 °C at pressures of 1.3-1.7 GPa. These P-T conditions are compatible with the selected isopleths and isomodes for the mineral phases considered in equilibrium with Grt_1 (X_{Mg}=0.92 for Cpx_{1b}, X_{Mg}=0.55 for Spl_1, and Spl_1 vol%=7, see Figures 7b, S1). Garnet isomodes are slightly overestimated but their trend suggests that the maximum vol% reached by Grt_1

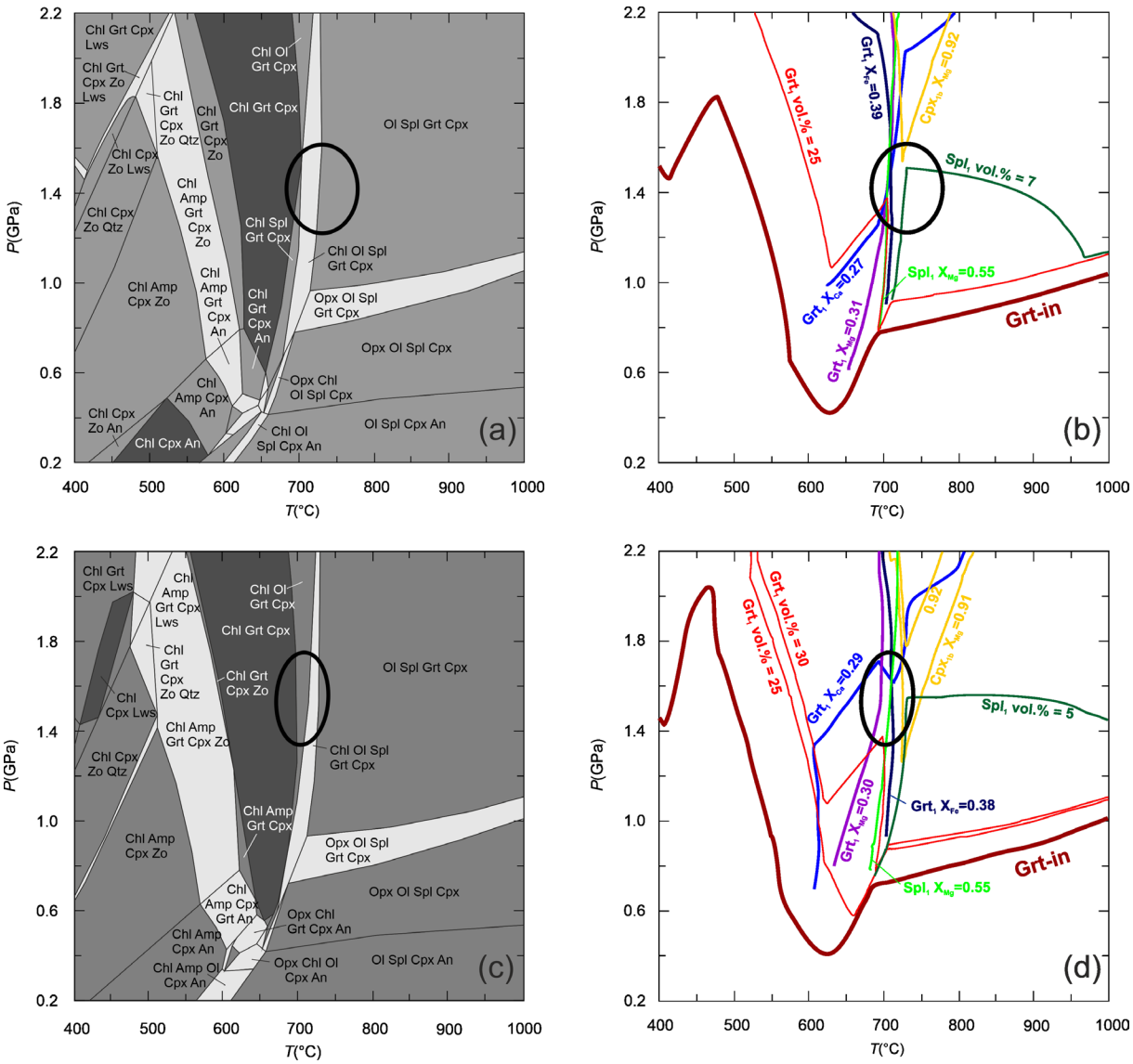

Figure 7. a) P-T pseudosection calculated in the CFMASH system for the effective composition of the coronitic domain of sample MNX (see section P-T Pseudosections for explanation). b) Estimated P-T conditions for the growth of the coronitic garnet in sample MNX. c) P-T pseudosection calculated in the CFMASH system for the effective composition of the coronitic domain of sample MNY. d) Estimated P-T conditions for the growth of the coronitic garnet in sample MNY. Mineral abbreviations as in Figure 4. Zo=zoisite. Lws=lawsonite; Qtz=quartz; An=anorthite. A few very small P-T fields are not assigned to a mineral assemblage.

corresponds to the peak pressure derived by Scodina et al. (2019). The obtained conditions relate to the P-T fields: (i) Ol+Spl+Grt+Cpx, (ii) Chl+ Ol+Spl+Grt+Cpx, (iii) Chl+ Grt+Cpx, and (iv) Chl+Spl+Grt+Cpx. These P-T fields have in common coexisting garnet and clinopyroxene, but differ for the presence of olivine, chlorite, and spinel (Figure 7 a,c). The P-T conditions obtained with the same approach for sample MNY are 1.4-1.8 GPa and 670-740 °C (Figure 7 c,d).

DISCUSSION OF THE P-T AND DISEQUILIBRIUM-EQUILIBRIUM CONDITIONS OF CORONITIC GARNET FORMATION

The thermobarometric data obtained by conventional thermobarometry and pseudosection modelling suggest that igneous crystallization occurred at P-T conditions <0.5 GPa and ca. 850 °C (Figure 8). Subsequently, the studied rocks underwent a progressive cooling phase accompanied by an increase in pressure (Scodina et al., 2019) compatible with garnet formation in microdomains. Cooling is further documented by the formation of coronitic microstructures, symplectites, and the exsolution of Fe-oxides from the host igneous orthopyroxene. The estimated peak pressure conditions of 1.3-1.7 GPa at temperatures of 680-730 °C (Figure 8) are very similar to those determined by Scodina et al. (2019) for a rock adjacent to the studied rocks. This demonstrates that (1) pseudosection modelling considering microdomains is a suitable method for deriving P-T conditions as previously suggested and (2) chemical equilibrium was reached at least at the microdomain scale despite the common prejudice that coronitic textures indicate disequilibrium conditions. In our samples, the slow reaction kinetics led to the formation of symplectitic/coronitic microstructures leaving a considerable portion of the earlier igneous phases. This also explains why symplectitic/coronitic microstructures in a specific rock do occur over considerable distances (meter range or even more) and are identical also in regard to the compositions of the minerals involved in the symplectitic microstructure.

CONCLUSIONS

The coronitic microstructures in the rocks of layer B from Mt. Nieddu record at least two main stages of metamorphic re-equilibration. The first stage is marked

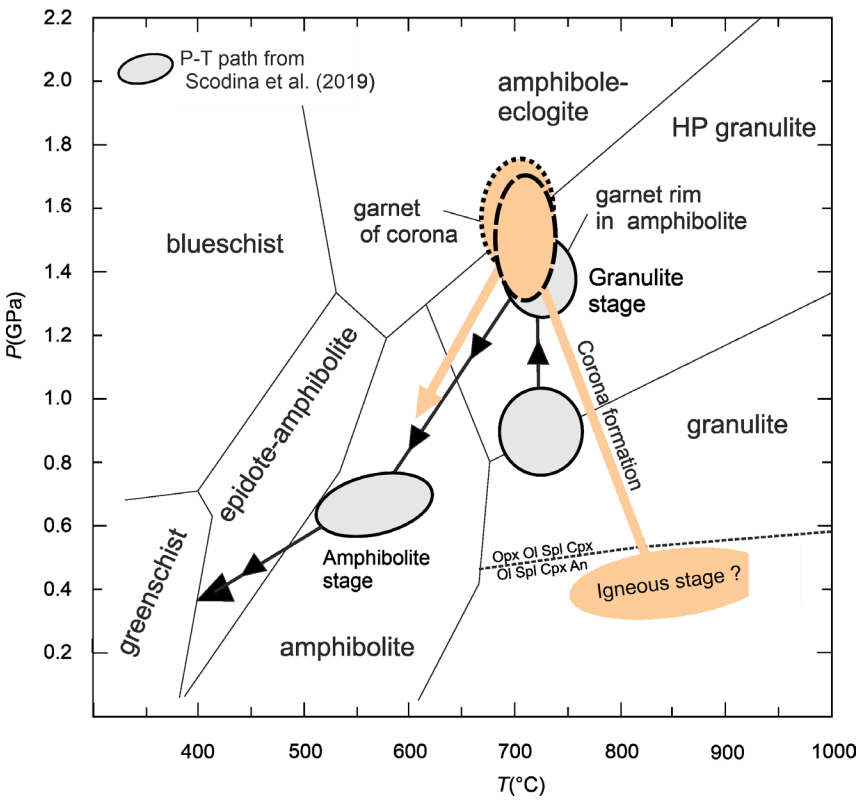

Figure 8. P-T conditions for igneous, granulite-facies, and amphibolite-facies stages and P-T path of the studied rocks from Mt. Nieddu (samples MNX and MNY, dotted black ellipses). Facies fields according to Liou et al. (1998).

by the formation of coronitic (Opx_1, Cpx_{1a}, and Cpx_{1b}, Spl_1 symplectite and later Grt_1) minerals at the expense of igneous olivine and plagioclase. The second stage, which led to the corona destabilization, is characterized by the overgrowth of amphiboles (Amp_{2a-b}) and the formation of spinel (Spl_2).

The applied pseudosection modelling for coronitic microdomains (formation of Grt_1) yielded HP granulite conditions of P=1.3-1.7 GPa at T=680-730 °C which are identical to those determined by Scodina et al. (2019) on an adjacent amphibolite. We conclude that chemical equilibrium was reached during corona formation probably over a much wider range than that of a single microdomain. The igneous phases remained because of slow reaction kinetics.

ACKNOWLEDGEMENTS

The authors are grateful to D. Castelli (University of Torino) and R. Cirrincione (University of Catania) for their helpful comments that improved the final version of the manuscript. The authors thank T. Theye who supported the EMP work at Universität Stuttgart. This work is part of the first author's Ph.D. thesis funded by Sardinia Regional Government (P.O.R. Sardegna F.S.E. Programme of the Autonomous Region of Sardinia, European Social Fund 2007-2013 - Axis IV Human Resources, Objective l.3, Line of Activity l.3.1.). Financial support was provided by Università di Cagliari and Regione Autonoma della Sardegna, L.R. 7/2007, research programme "Il blocco Sardo-Corso: area chiave per la ricostruzione della geodinamica varisica" CUP J81G17000110002.

REFERENCES

Anderson A.T., 1968. Oxidation of the La Blanche Lake titaniferous magnetite deposit, Québec. The Journal of Geology 76, 528-547.

Barca S., Carmignani L., Eltrudis A., Franceschelli M., 1995. Origin and evolution of the Permian-Carboniferous basin of Mulargia Lake (South-Central Sardinia, Italy) related to the Late-Hercynian extensional tectonic. Comptes Rendus de l'Académie des Sciences Paris 321 (IIa), 171-178.

Bethume K.M. and Davidson A., 1997. Grenvillian metamorphism of the Sudbury diabase dyke-swarm: from protolith to two-pyroxene-garnet coronite. The Canadian Mineralogist 35, 1191-1220.

Brandelik A., 2009. CALCMIN - an EXCELTM Visual Basic application for calculating mineral structural formulae from electron microprobe analyses. Computers & Geosciences 35, 1540-1551.

Brey G.P. and Köhler T., 1990. Geothermobarometry in four-phase lherzolites II. New thermobarometers, and practical assessment of existing thermobarometers. Journal of Petrology 31, 1353-1378.

Burnham C.W., Holloway J.R., Davis N.F., 1969. Thermodynamic properties of water to 1,000 °C and 10,000 bars. Geological Society of America Special Paper 132, 96.

Cappelli B., Carmignani L., Castorina F., Di Pisa A., Oggiano G., Petrini R., 1992. A Variscan suture zone in Sardinia: geological, geochemical evidence, Paleozoic Orogenies in Europe (special issue). Geodinamica Acta 5, 101-118.

Carmignani L., Carosi R., Di Pisa A., Gattiglio M., Musumeci G., Oggiano G., Pertusati P.C., 1994. The Hercynian chain in Sardinia (Italy). Geodinamica Acta 5, 217- 233.

Carmignani L., Oggiano G., Barca S., Conti P., Eltrudis A., Funedda A., Pasci S., Salvadori I., 2001. Geologia della Sardegna. Note illustrative della Carta Geologica della Sardegna in scala 1:200,000. Memorie descrittive della Carta Geologica d'Italia LX, 283.

Carosi R., Frassi C., Iacopini D., Montomoli C., 2005. Post collisional transpressive tectonics in northern Sardinia (Italy). Journal of the Virtual Explorer 19, paper 3.

Carosi R. and Palmeri R., 2002. Orogen-parallel tectonic transport in the Variscan belt of northeastern Sardinia (Italy): implications for the exhumation of medium-pressure metamorphic rocks. Geological Magazine 139, 497-511.

Connolly J.A.D., 1990. Multivariable phase diagrams: an algorithm based on generalized thermodynamics. American Journal of Sciences 290, 666-718.

Connolly J.A.D., 2009. The geodynamic equation of state: what and how. Geochemistry, Geophysics, Geosystems 10, Q10014.

Connolly J.A.D., Memmi I., Trommsdorff V., Franceschelli M., Ricci C.A., 1994. Forward modelling of Ca-silicate microinclusion and fluid evolution in a graphitic metapelite (NE Sardinia). American Mineralogist 79, 960-972.

Corsi B. and Elter F.M., 2006. Eo-Variscan (Devonian?) melting in the High-Grade Metamorphic Complex of the NE Sardinia Belt (Italy). Geodinamica Acta 19, 155-164.

Cruciani G., Dini A., Franceschelli M., Puxeddu M., Utzeri D., 2010. Metabasite from the Variscan belt in NE Sardinia, Italy: within-plate OIB-like melts with very high Sr and low Nd isotope ratios. European Journal of Mineralogy 22, 509-523.

Cruciani G., Fancello D., Franceschelli M., Scodina M., Spano M.E., 2014a. Geothermobarometry of Al-silicate bearing migmatites from the Variscan chain of NE Sardinia, Italy: a P-T pseudosection approach. Periodico di Mineralogia 83, 19-40.

Cruciani G., Franceschelli M., Foley S.F., Jacob D.E., 2014b. Anatectic amphibole and restitic garnet in Variscan migmatite from NE Sardinia, Italy: insights into partial melting from mineral trace elements. European Journal of Mineralogy 26, 381-395.

Cruciani G., Franceschelli M., Groppo C., 2011. P-T evolution of eclogite-facies metabasite from NE Sardinia, Italy: insights into the prograde evolution of Variscan eclogites. Lithos 121, 135-150.

Cruciani G., Franceschelli M., Groppo C., Oggiano G., Spano

M.E., 2015a. Re-equilibration history and P-T path of eclogites from Variscan Sardinia, Italy: a case study from the medium-grade metamorphic complex. International Journal of Earth Sciences 104, 797-814.

Cruciani G., Franceschelli M., Groppo C., Spano M.E., 2012. Metamorphic evolution of non-equilibrated granulitized eclogite from Punta de li Tulchi (Variscan Sardinia) determined through texturally controlled thermodynamic modeling. Journal of Metamorphic Geology 30, 667-685.

Cruciani G., Franceschelli M., Marchi M., Zucca M., 2002. Geochemistry of metabasite from NE Sardinia, Italy: nature of protoliths, magmatic trend, and geotectonic setting. Mineralogy and Petrology 74, 25-47.

Cruciani G., Franceschelli M., Massonne H.-J., Carosi R., Montomoli C., 2013. Pressure-temperature and deformational evolution of high-pressure metapelites from Variscan NE Sardinia, Italy. Lithos 175-176, 272-284.

Cruciani G., Franceschelli M., Langone A., Puxeddu M., Scodina M., 2015b. Nature and age of pre-Variscan eclogite protoliths from the low- to medium-grade metamorphic complex of north-central Sardinia (Italy) and comparison with coeval Sardinian eclogites in the northern Gondwana context. Journal of the Geological Society 172, 792-807.

Cruciani G., Montomoli C., Carosi R., Franceschelli M., Puxeddu M., 2015c. Continental collision from two perspectives: A review of Variscan metamorphism and deformation in northern Sardinia. Periodico di Mineralogia 84, 657-699.

Dale J., Powell R., White R.W., Elmer F.L., Holland T.J.B., 2005. A thermodynamic model for Ca-Na clinoamphiboles in Na_2O-CaO-FeO-MgO-$Al_2$2O_3-SiO_2-H_2O-O for petrological calculations. Journal of Metamorphic Geology 23, 771-791.

Di Vincenzo G., Carosi R., Palmeri R., 2004. The relationship between tectono-metamorphic evolution and argon isotope records in white mica: constraints from in situ ^{40}Ar-^{39}Ar laser analysis of the Variscan basement of Sardinia. Journal of Petrology 45, 1013-1043.

Doukkari S.A., Ouzegane K., Godard G., Diener J.F.A., Kienast J.R., Liégeois J.P., Arab A., Drareni A., 2015. Prograde and retrograde evolution of eclogite from Adrar Izzilatène (Egéré-Aleksod terrane, Hoggar, Algeria) determined from chemical zoning and pseudosections, with geodynamic implications. Lithos 226, 217-232.

Ellis D.J. and Green D.H., 1979. An experimental study of the effect of Ca upon garnet-clinopyroxene Fe -Mg exchange equilibria. Contributions to Mineralogy and Petrology 71, 13-22.

Elter F.M., Padovano M., Kraus R.K., 2010. The Variscan HT metamorphic rocks emplacement linked to the interaction between Gondwana and Laurussia plates: structural constraints in NE Sardinia (Italy). Terra Nova 22, 369-377.

Fancello D., Cruciani G., Franceschelli M., Massonne H.-J., 2018. Trondhjemitic leucosomes in paragneisses from NE Sardinia: Geochemistry and P-T conditions of melting and crystallization. Lithos 304-307, 501-517.

Ferrara G., Rita F., Ricci C.A., 1978. Isotopic age and tectonometamorphic history of the metamorphic basement of North-Eastern Sardinia. Contributions to Mineralogy and Petrology 68, 99-106.

Franceschelli M., Carcangiu G., Caredda A.M., Cruciani G., Memmi I., Zucca M., 2002. Transformation of cumulate mafic rocks to granulite and re-equilibration in amphibolite and greenschist facies in NE Sardinia, Italy. Lithos 63, 1-18.

Franceschelli M., Puxeddu M., Cruciani G., 2005a. Variscan metamorphism in Sardinia, Italy: review and discussion. Journal of the Virtual Explorer 19, paper 2.

Franceschelli M., Puxeddu M., Cruciani G., Utzeri D., 2007. Metabasites with eclogite facies relics from Variscides in Sardinia, Italy: a review. International Journal of Earth Science 96, 795-815.

Gaidies F., Milke R., Heinrich W., Abart R., 2017. Metamorphic mineral reactions: porphyroblast, corona and symplectite growth. EMU notes in Mineralogy 16, 469-540.

Gattacecca J., 2001. Cinématique du bassin Liguro-Provençal entre 30 et 12 Ma: Implications géodynamiques. Mémoires des sciences de la Terre, Ecole des mines de Paris 41, 299.

Ghezzo C., Memmi I., Ricci C.A., 1979. Un evento granulitico nel basamento metamorfico della Sardegna nord-orientale. Memorie della Società Geologica Italiana 20, 23-38.

Green E.C.R., Holland T.J.B., Powell R., 2007. An order-disorder model for omphacitic pyroxenes in the system jadeite-diopside-hedenbergite-acmite with applications to eclogitic rocks. American Mineralogist 92, 1181-1189.

Groppo C., Rolfo F., Liu Y.C., Deng L.P., Wang A.D., 2015. P-T evolution of elusive UHP eclogites from the Luotian dome (North Dabie Zone, China): How far can the thermodynamic modeling lead us? Lithos 226, 183-200.

Groppo C., Lombardo B., Castelli D., Compagnoni R., 2007. Exhumation history of the UHPM Brossasco-Isasca Unit, Dora-Maira Massif, as inferred from a phengite-amphibole eclogite. International Geology Review 49, 142-168.

Helgeson H.C., Delaney J.M., Nesbitt H.W., Bird D.K., 1978. Summary and critique of the thermodynamic properties of rock-forming minerals. American Journal of Sciences 278A, 229.

Holland T.J.B., Baker J.M., Powell R., 1998. Mixing properties and activity-composition relationships of chlorites in the system MgO-FeO-Al_2O_3-SiO_2-H_2O. European Journal of Mineralogy 10, 395-406.

Holland T.J.B. and Powell R., 1996. Thermodynamics of order-disorder in minerals, 2. Symmetric formalism applied to solid solutions. American Mineralogist 81, 1425-1437.

Holland T.J.B. and Powell R., 1998. An internally consistent thermodynamic data set for phases of petrological interest. Journal of Metamorphic Geology 16, 309-343.

Jašarová P., Racek M., Jeřábek P., Holub F.V., 2016. Metamorphic reactions and textural changes in coronitic metagabbros

from the Teplá Crystalline and Mariánské Lázně complexes, Bohemian Massif. Journal of Geosciences 61, 193-219.

Korzhinskii D., 1959. Physicochemical basis of the analysis of the paragenesis of minerals. Consultants Bureau, New York, USA. 142 pp.

Leake B.E., Woolley A.R., Arps C.E.S., Birch W.D., Gilbert M.C., Grice J.D., Hawthorne F.C., Kato A., Kisch H.J., Krivivichev V.G., Linthout K., Laird J., Mandarino J.A., Maresch W.V., Nickel E.H., Rock N.M.S., Schumacher J.C., Smith D.C., Stephenson N.C.N., Ungaretti L., Whittaker E., Youzhi G., 1997. Nomenclature of amphiboles: report of the subcommittee on amphiboles of the International Mineralogical Association, commission on new minerals and mineral names. European Journal of Mineralogy 9, 623-651.

Lindsley D.H. and Spencer K.J., 1982. Fe-Ti oxide geothermometry: Reducing analyses of coexisting Ti-magnetite (Mt) and ilmenite (Ilm) abstract AGU 1982 Spring Meeting Eos Transactions. American Geophysical Union 63, 471.

Liou J.G., Zhang R.Y., Ernst W.G., Rumble D. III, Maruyama S., 1998. High-pressure minerals from deeply subducted metamorphic rocks. In: Ultrahigh-Pressure Mineralogy (ed. Hemley, R.J.) Reviews in Mineralogy 37, 33-96.

Massonne H.-J., 2012. Formation of amphibole and clinozoisite-epidote in eclogite owing to fluid infiltration during exhumation in a subduction channel. Journal of Petrology 53, 1969-1998.

Massonne H.-J., Cruciani G., Franceschelli M., 2013. Geothermobarometry on anatectic melts - a high-pressure Variscan migmatite from northeast Sardinia. International Geology Review 55, 1490-1505.

Massonne H.-J., Cruciani G., Franceschelli M., Musumeci G., 2018. Anticlockwise pressure-temperature paths record Variscan upper-plate exhumation: example from micaschists of the Porto Vecchio region, Corsica. Journal of Metamorphic Geology 36, 55-77.

Newton R.C., Charlu T.V., Kleppa O.J., 1981. Thermochemistry of the high structural state plagioclases. Geochimica et Cosmochimica Acta 44, 933-941.

Padovano M., Elter F.M., Pandeli E., Franceschelli M., 2012. The East Variscan Shear Zone: new insights into its role in the Late Carboniferous collision in southern Europe. International Geology Review 54, 957-970.

Powell R., 1985. Regression diagnostics and robust regression in geothermometer/geobarometer calibration: the garnet-clinopyroxene geothermometer revisited. Journal of Metamorphic Geology 2, 231-243.

Powell R. and Holland T., 1999. Relating formulations of the thermodynamics of mineral solid solutions: activity modeling of pyroxenes, amphiboles, and micas. American Mineralogist 84, 1-14.

Powell R. and Holland T.J.B., 2008. On thermobarometry. Journal of Metamorphic Geology 26, 155-179.

Putirka K.D., 2008. Thermometers and barometers for volcanic systems. Reviews in Mineralogy and Geochemistry 69, 61-120.

Scodina M., Cruciani G., Franceschelli M., Massonne H.-J., 2019. Anticlockwise P-T evolution of amphibolites from NE Sardinia, Italy: geodynamic implications for the tectonic evolution of the Variscan Corsica-Sardinia block. Lithos 324-325, 763-775.

Séranne M., 1999. The Gulf of Lion continental margin (NW Mediterranean) revisited by IBS: an overview. Geological Society of London, Special Publication 156, 15-36.

Stormer Jr. J.C., 1983. The effects of recalculation on estimates of temperature and oxygen fugacity from analyses of multi-component iron-titanium oxides. American Mineralogist 68, 586-594.

Thompson J.B., 1959. Local equilibrium in metasomatic processes. In: Researches in Geochemistry, 1 (P.H. Abelson, editor). Wiley, New York, pp. 427-457.

Torres-Roldan R.L., Garcia-Casco A., Garcia-Sanchez P.A., 2000. CSpace: an integrated workplace for the graphical and algebraic analysis of phase assemblages on 32-bit wintel platforms. Computers & Geosciences 26, 779-793.